ADVANCED MATERIALS
www.advmat.de

Triboelectrification-Enabled Self-Powered Detection and Removal of Heavy Metal Ions in Wastewater

Zhaoling Li, Jun Chen, Hengyu Guo, Xing Fan, Zhen Wen, Min-Hsin Yeh, Chongwen Yu, Xia Cao, and Zhong Lin Wang**

Unlike organic contaminants, heavy metal ions are not biodegradable and tend to accumulate in living organisms.[1] Most of them are known to be toxic or carcinogenic, and thus, impose a threat to human life and health. Nowadays, increasing amounts of various heavy metal ions extensively exist in the wastewater due to the rapid development of industries such as metal plating facilities, mining operations, fertilizer industries, batteries, paper industries, and pesticides, which widely jeopardize not only the ambient ecosystems but also the health of human beings.[2–4] The treatment of heavy metals is of special concern due to their recalcitrance and persistence in the environment, which also places a permanent damage to the underground water system once invaded.[5]

In recent years, increased efforts have been committed to detect and remove the heavy metal ions from the ambient environments, especially from the discharged industrial wastewater. For the time being, techniques for heavy metal ions treatment are limited to inductively coupled plasma-optical emission spectroscopy, inductively coupled plasma-mass spectrometry, atomic absorption spectrometer, X-ray fluorescence spectrometry, chemical precipitation, reverse osmosis, ion exchange, membrane filtration, coagulation–flocculation, and electrochemical methods.[6–10] Widespread usage of these techniques is likely to be shadowed by possible limitations, such as sophisticated and expensive equipment, complicated and time-consuming procedures, high energy consumption, highly trained technicians to perform and reliance on external power sources.[11–13]

Here, we introduce a fundamentally new working principle to the field of heavy metal ion treatment by reporting a unique route that works in a self-powered manner by harnessing the ambient energy using the triboelectrification effect. Relying on modified anodic aluminum oxide (AAO) a nanoporous surface with a layer of appropriate ligand molecules, serving as recognition element, the as-developed tribo-nanosensors can selectively capture and detect Cu^{2+}, Pb^{2+}, and Cr^{3+}, which are commonly existing toxic heavy metal ions in industrial wastewater, in a sensing range of 0–200 $\times$ 10^{-6} M with a sensitivity of 0.005 $\times$ 10^{-6}, 0.003 $\times$ 10^{-6}, and 0.004 $\times$ 10^{-6} M^{-1}, respectively. The presented tribo-nanosensors are also proved to possess good stability after continuous working for up to 50,000 cycles. Moreover, the ambient triboelectrification effect was further utilized to develop a water-driven triboelectric nanogenerator (WD-TENG) as a sustainable power source for heavy metal ion removal by recycling the kinetic energy from flowing wastewater. The self-provided electric field can boost the migration and combination of ions as well as the electrolysis effect. The later induced a generation of large amount of OH^- at the cathode in the wastewater, which promoted the precipitation of heavy metal ions. By controlling the wastewater pH values, Cu^{2+}, Pb^{2+}, and Cr^{3+} were demonstrated to be fractionally precipitated from the wastewater. Under a fixed water flow rate of 3 L min^{-1} and initial heavy metal ion concentration of 100 $\times$ 10^{-6} M, the self-powered cleaning system was capable of removing 97.4% of the heavy metal ions in the wastewater in 100 min. In addition, a further step was taken to recycle and collect the precipitated metals. Through a filtration, acidification, and chemical reduction process, pure metals are respectively obtained, which realizes the clean production and recycling economy.

Featured as high detection sensitivity and removal efficiency, cost-effectiveness, simplicity as well as stability, the reported work not only opens a new and innovative pathway to environmentally friendly treatment of the ambient heavy metal ions, but also promotes substantial advancements in the fields of clinical toxicology, immunological surveillance, environmental monitoring, industrial waste management, and recycling economy.

The triboelectrification enabled self-powered heavy metal ion treatment systematically consists of two steps, a tribo-nanosensor for metal ion detection and a water-driven triboelectric nanogenerator for metal ion removal. As demonstrated in **Figure 1**a, the as-developed tribo-nanosensor holds a multilayered structure with acrylic as supporting substrates. On the upper substrate, a layer of polytetrafluoroethylene (PTFE) film was adhered as one contact surface with back-coated copper as the electrode. PTFE nanowires arrays were created on the exposed PTFE surface by a top–down method through

Z. Li, J. Chen, H. Guo, Dr. X. Fan, Z. Wen,
Dr. M.-H. Yeh, Prof. Z. L. Wang
School of Materials Science and Engineering
Georgia Institute of Technology
Atlanta, GA 30332-0245, USA
E-mail: zlwang@gatech.edu
Z. Li, Prof. C. Yu
Key Laboratory of Science and Technology of Eco-Textiles
Ministry of Education
College of Textiles
Donghua University
Shanghai 201620, P. R. China
Prof. X. Cao, Prof. Z. L. Wang
Beijing Institute of Nanoenergy and Nanosystems
Chinese Academy of Sciences
Beijing 100083, P. R. China
E-mail: caoxia@binn.cas.cn

DOI: 10.1002/adma.201504356

ADVANCED MATERIALS
www.advmat.de

www.MaterialsViews.com

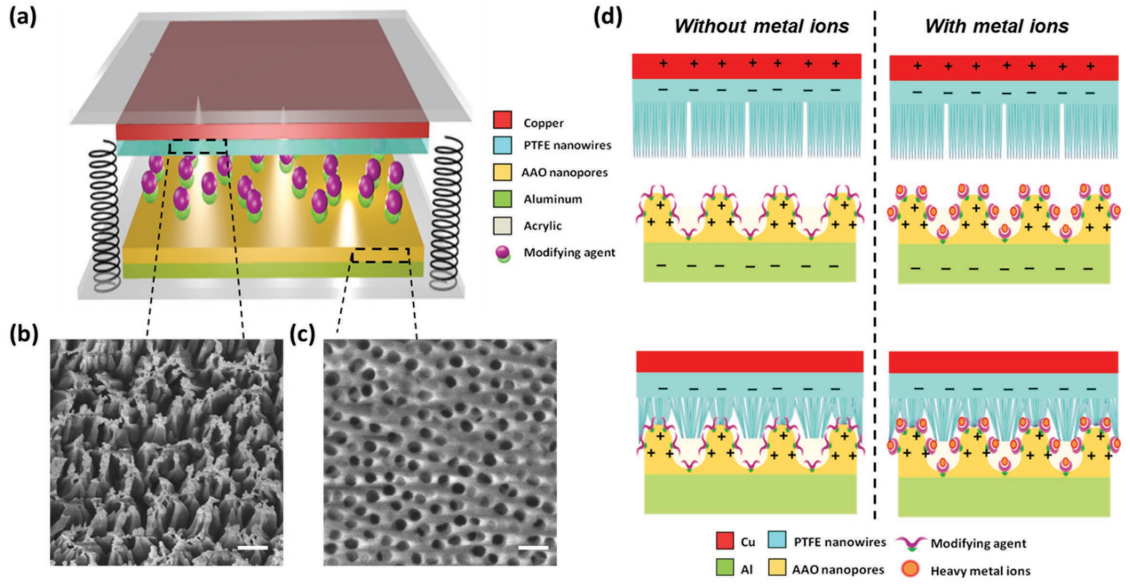

Figure 1. Structure design and working principle of the as-developed tribo-nanosensor for heavy metal ion detection. a) A sketch showing the structural design of the tribo-nanosensor. b) An SEM image of the PTFE nanowires. The scale bar is 200 nm. c) A SEM image of the anodic aluminum oxide nanopores. The scale bar is 500 nm. d) Schematic diagram of the working principle of the tribo-nanosensor for heavy metal ion detection, which consists of a triboelectrification and a complexation reaction process.

reactive ion etching. A scanning electron microscopy (SEM) image of the PTFE nanowires is displayed in Figure 1b, which indicates an average diameter of 34 ± 3 nm and an average length of 1.1 ± 0.4 μm. On the lower substrate, a layer of Al foil with surface grown AAO nanopores is laminated as another contact surface. An SEM image of the nanopores is presented in Figure 1c. The nanopores were uniformly distributed on the aluminum surface with an average diameter of 80 ± 5 nm and a pore depth of 40 ± 10 nm with a distribution density of 210 μm^{-2}. And the corresponding X-ray diffraction (XRD) pattern of AAO nanopores is shown in Figure S1 in the Supporting Information. A detailed fabrication process of the tribo-nanosensor is presented in the Experimental Section.

The working principle of the tribo-nanosensor for heavy metal ion detection is schematically illustrated in Figure 1d, which can be elucidated in two aspects, namely, ligand molecules as surface chemical modifications and triboelectrification for heavy metal ion detection.[14–21] To operate, AAO nanopores were first chemically modified with appropriate ligand molecules via physical adsorption, which enables the AAO nanopores to possess good chelating properties toward different metal ions. These modifying ligand molecules are capable of selectively adsorbing the heavy metal ions as their recognizing elements. A difference of the complexation constant between heavy metal ions and ligand molecules contributes to a different affinity to the metal ions.[2,4] Chemically, a higher complexation will lead to a stronger ability of metal ions adsorption, while very limited amount of metal ions can be adsorbed in the presence of a weak complexation. For the sensing, the adsorbed metal ions on the AAO surface will highly influence the electric output of the as-developed tribo-nanosensor. Since an increasing amount of metal ions will gradually reduce the triboelectrication between the PTFE nanowires and the AAO nanopores, and thus the acquired electric output of the tribo-nanosensor. Subsequently, by analyzing the electric output signals of the as-fabricated tribo-nanosensor, the detection of the heavy metal ions can be realized. Here, AAO is selected owing to its relatively high adsorption capacity, strong mechanical structure, and more importantly, low cost and easy fabrication.

An illustration of the electricity generation process is presented in Figure S2 in the Supporting Information. At the original position, an initial contact of AAO with the PTFE brought about charges transfer due to their different electron affinity, resulting in positive charges on the AAO and negative ones on the PTFE (Figure S2a, Supporting Information). Once separation emerges, the induced electrical potential difference drives the electrons to flow from Cu electrode to Al electrode (Figure S2b, Supporting Information). With continuously increasing the separation between the two electrodes, almost all of the positive triboelectric charges are screened (Figure S2c, Supporting Information). As the two plates are approaching each other due to the spring elastic force, electrons are driven back from Al electrode to Cu electrode (Figure S2d, Supporting Information).[22–33] Given a consistent and cyclical operation of the two plates of the as-fabricated tribo-nanosensor at a fixed surface concentration of modifying agent, the acquired output electric signals in the external circuit are correlated to the surface adsorbed heavy metal ion concentrations on the AAO nanopores.

To demonstrate the capability of the as-developed tribo-nanosensor for heavy metal ion detection, Pb^{2+}, Cr^{3+}, Cu^{2+} were selected for the test due to their high toxicity and common existence in the industrial wastewater. And dithizone, diphenylcarbazide, and sodium diethyldithiocarbamate were assembled onto the AAO nanopores as recognition marks for Pb^{2+}, Cr^{3+}, and Cu^{2+}, respectively.

Adv. Mater. **2016**,
DOI: 10.1002/adma.201504356

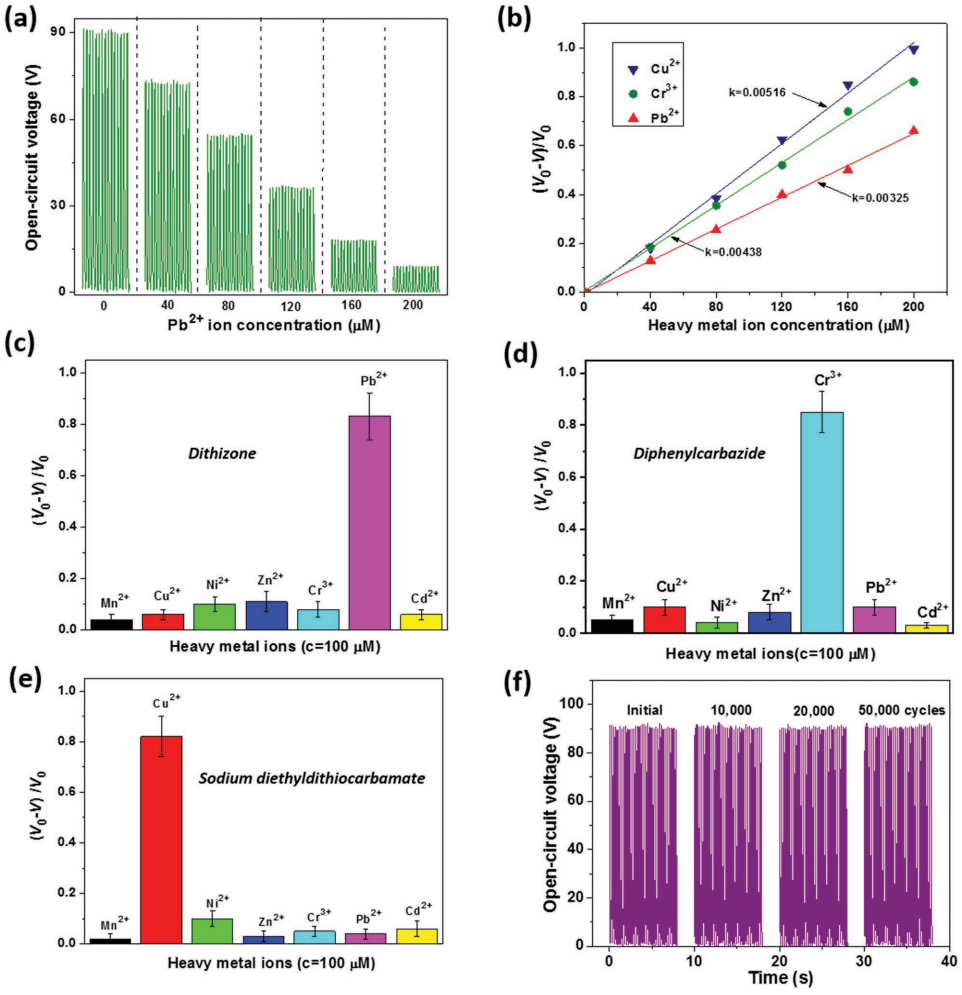

Figure 2. Performance characterization of the tribo-nanosensor for heavy metal ion detection. a) Dependence of the open-circuit voltage of the tribo-nanosensor on the Pb^{2+} concentration, under a fixed amount of the dithizone molecules as the surface modifying agent. b) Tests of the sensitivity of the as-developed tribo-nanosensor for Pb^{2+}, Cu^{2+}, Cr^{3+} heavy metal detection. c) Test of the selectivity of the as-developed tribo-nanosensor for Pb^{2+} detection by using the dithizone as the surface modifying agent. d) Test of the selectivity of the as-developed tribo-nanosensor for Cr^{3+} detection by using the diphenylcarbazide as the surface modifying agent. e) Test of the selectivity of the as-developed tribo-nanosensor for Cu^{2+} detection by using the sodium diethyldithiocarbamate as the surface modifying agent. f) A test of the stability of the as-developed tribo-nanosensor for heavy metal ion detection.

Experimentally, heavy metal ion solutions with various concentrations but constant volumes of 20 μL were dropped onto the modified AAO nanopores surface after being modified by its corresponding agent with a fixed concentration of 100 μM. A drying process at ambient temperature was performed before a further electrical measurement. The dependence of the open-circuit voltage output on the Pb^{2+} concentration is presented in **Figure 2**a. In a certain Pb^{2+} concentration region of 0 to 200 × 10^{-6} M, the open-circuit voltage is a monotonically decreasing function of the Pb^{2+} concentrations throughout the experimental time windows. The dependence of short-circuit current output on the Pb^{2+} concentrations was also investigated and the results were presented in Figure S3 in the Supporting Information, showing the same trend. A decrease of the electric output is mainly attributed to the surface-adsorbed Pb^{2+} molecules, which will partially replace the position of AAO to contact with PTFE. Given a lower tendency of the Pb^{2+} molecules to lose electrons, a decrease of the electric output is thus observed with the increasing of the Pb^{2+} concentrations. Likewise, Cu^{2+} and Cr^{3+} exhibited similar changing trends between the electric output and the applied concentration. The sensing performance of the tribo-nanosensor for heavy metal ion detection was evaluated in terms of open-circuit voltage ratio ($(V_0-V)/V_0$), as shown in Figure 2b. The experimental observations reveal that the tribo-nanosensor is capable of effectively detecting the applied Cu^{2+}, Pb^{2+}, and Cr^{3+} in a sensing range of 0–200 × 10^{-6} M. More notably, in a self-powered working manner, a superior sensitivity of 0.005 × 10^{-6}, 0.003 × 10^{-6}, and 0.004 × 10^{-6} M^{-1} was achieved toward the ambient Cu^{2+}, Pb^{2+}, and Cr^{3+} detection, respectively.

As a critical feature of a sensor, the selectivity of the as-developed tribo-nanosensor was further explored. In this regard, first, a set of control experiments were carried out toward Pb^{2+} detection. To start, the tribo-nanosensors were treated with dithizone as the modifying agent and Pb^{2+} recognition element. As shown in Figure 2c, under the same testing condition, the open-circuit voltage ratio of the tribo-nanosensor

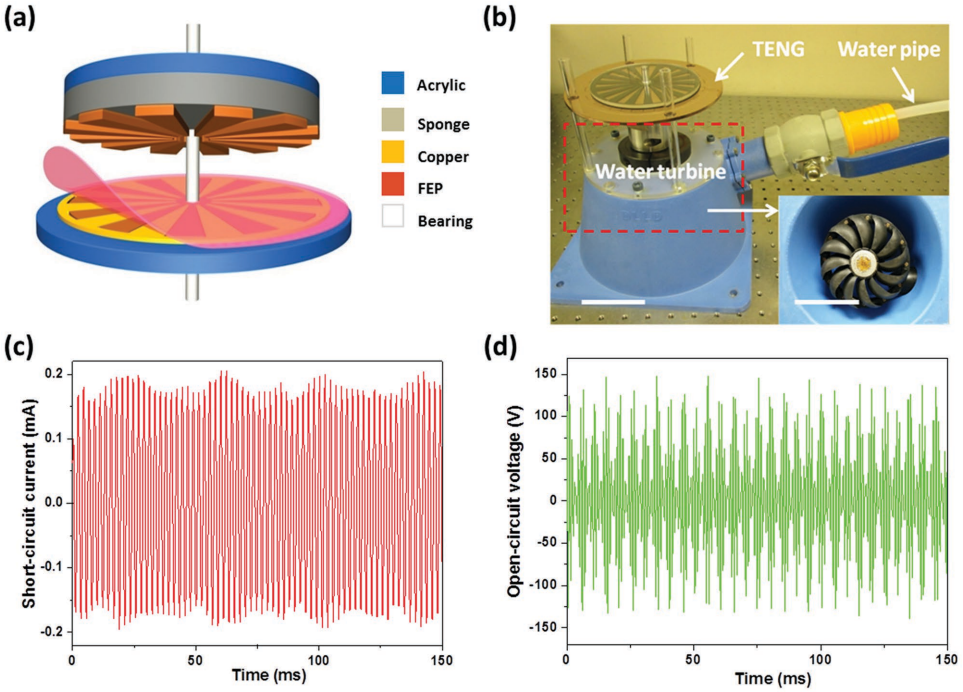

Figure 3. A water-driven triboelectric nanogenerator (WD-TENG) for heavy metal ion removal. a) Structural design of the WD-TENG. b) A photograph of the experimental setup showing the WD-TENG as a sustainable power source for heavy metal ion removal by recycling the waste water flow energy. The inset shows an inside view of the water turbine. The scale bars are 5 cm. c) The short-circuit current and (d) the open-circuit voltage of the WD-TENG under a fixed water flow rate of 3 L min^{-1}.

with Pb^{2+} absorption was far larger than that for other heavy metal ions, which indicated an excellent selectivity of the tribo-nanosensor for Pb^{2+} detection. Likewise, being respectively treated with diphenylcarbazide and sodium diethyldithiocarbamate, the tribo-nanosensors were also showing remarkable selectivity toward Cr^{3+} and Cu^{2+} detection, as demonstrated in Figure 2d,e.

For a systematic investigation, a further step was taken to evaluate the stability of tribo-nanosensor for heavy metal ion detection. To perform it, an electrodynamic shaker (from Labworks Inc.) that provides a sinusoidal wave was used as an impact source to operate the tribo-nanosensor. After a 50,000-cycle continuous operation, no degradation of the electric output was observed, as shown in Figure 2f, indicating a good stability of the device. Featured as high sensitivity, selectivity, and stability, the reported tribo-nanosensor represented a self-powered technique, which could also be extensively applied to other heavy metal ion detection.

Besides, the absorbed ligand molecules such as dithizone, diphenylcarbazide, sodium diethyldithiocarbamate can be removed completely by 20 mL ethyl alcohol rinsing from the AAO surface. Both SEM images (Figure S4a,b, Supporting Information) and the XRD patterns (Figure S4c, Supporting Information) show no surface morphology or chemical composition change after the refurbishment. Furthermore, as shown in Figure S4d in the Supporting Information, there is also no observable output degradation of the measured open-circuit voltage for the refurbished tribo-nanosensor. These observations prove a good reusability of the device for heavy metal ion detection.

For a systematic treatment of the ambient heavy metal ions, a further action was taken to remove the heavy metal ions after being detected. Here, a WD-TENG was developed to recycle the kinetic energy of flowing waste water,[34–43] acting as a self-generated electric field to enhance the hydroxide precipitation of heavy metal ions. The as-fabricated device's dimension is 10 cm × 10 cm × 1.5 mm. The structural design of the WD-TENG is shown in **Figure 3**a, which consists of mainly two parts: A rotator and a stator. The rotator is a collection of radially arrayed sectors with a unit central angle of 6°. The stator comprises three components: A layer of fluorinated ethylene propylene (FEP) as an electrification material, a layer of electrodes with complementary patterns, and an underlying substrate laminated along the vertical direction. Photographs of the as-fabricated stator and rotator of the WD-TENG were demonstrated in Figure S5 in the Supporting Information. Detailed fabrication process and description of the working principle of the WD-TENG were respectively presented in the Experimental Section and Figure S6 in the Supporting Information. Also, the detailed electricity-generating process was elaborated through a basic unit in Figure S7 and Figure S8 in the Supporting Information. The corresponding description can be found in the Supporting Information.

Experimentally, to demonstrate the working principle, the WD-TENG was connected to the central shaft of a miniature water turbine. Normal tap water was directed into the turbine inlet through a plastic pipe. A photograph of the experimental setup was shown in Figure 3b. Under a fixed water flow rate of 3 L min^{-1}, the output voltage and current were respectively plotted in Figure 3c,d. As shown, the short-circuit current

Adv. Mater. **2016**,
DOI: 10.1002/adma.201504356

(I_{sc}) has a continuous AC output with an average amplitude of 0.18 mA. And the open-circuit voltage (V_{oc}) oscillates at the same frequency as that of I_{sc} with a peak-to-peak value of 310 V. The efficiency of the WD-TENG is defined as the ratio of the generated electricity to the flowing kinetic energy from water turbine. And this energy conversion efficiency is calculated to be ≈12.7%. A detailed calculation is presented in Note S1 in the Supporting Information. It is important to note that discharging pipes or sewages widely exist in the wastewater pool, where contains plenty of kinetic flowing energy and can be harnessed to convert into electricity by the WD-TENG. Furthermore, when a wind passed across the waste water surface, the aroused water wave can also be harnessed by the WD-TENG.

To characterize the performance of the reported approach for heavy metal ion removal, experimentally, $CuSO_4$, $Pb(NO_3)_2$, and $CrCl_3$ were dissolved in tap water to mimic the ambient wastewater samples with a controlled amount of anions and cations. Referring to the standard water quality testing conditions,[44,45] the wastewater samples were prepared, as the characteristics shown in Table S1 in the Supporting Information. And a schematic diagram of the working principle of the integrated self-powered system for heavy metal ion cleaning is presented in **Figure 4**. The whole self-powered system consisted of a WD-TENG for power supply, a rectifier unit and a chemical reaction pond with industrial wastewater, as demonstrated in Figure 4a. Two pieces of graphite acting as cathode and anode were immersed in the reaction pond. And a pH controller was employed to monitor the pH values in the reaction solution. The detailed fabrication and experimental setup of the self-powered integration system is presented in the Experimental Section. To illustrate the working mechanism of the self-provided electric field for the acceleration of heavy metal ion precipitation, two sketches were respectively employed, as shown, the ions hydroxide precipitation process without (Figure 4b) and with (Figure 4c) the assistance of an applied electric field. In the precipitation process, the soluble heavy metals ions will precipitate at certain pH value.[10,11] The self-provided electric field can promote the directed migration of the ions, which is called electrophoresis, in the integrated electrochemical system. The cations move toward the cathode, while the anions move toward the anode under the influence of the applied electric field. In the meanwhile, the self-provided electric filed can boost the electrolysis effect and induce the generation of large amount of OH^- at the cathode in the wastewater, which largely promoted the heavy metal ion precipitation. By controlling the wastewater pH values, Cu^{2+}, Pb^{2+}, and Cr^{3+} were demonstrated to be fractionally precipitated from the wastewater. The formed precipitates can be further separated and removed from the water by sedimentation or filtration.

UV–vis spectroscopy can be routinely used in analytical chemistry for quantitative determination of different analyses. Here, in order to prove the effectiveness of this method for heavy metal ion detection, a detection sensitivity comparison of the UV–vis spectrophotometer and Inductively Coupled

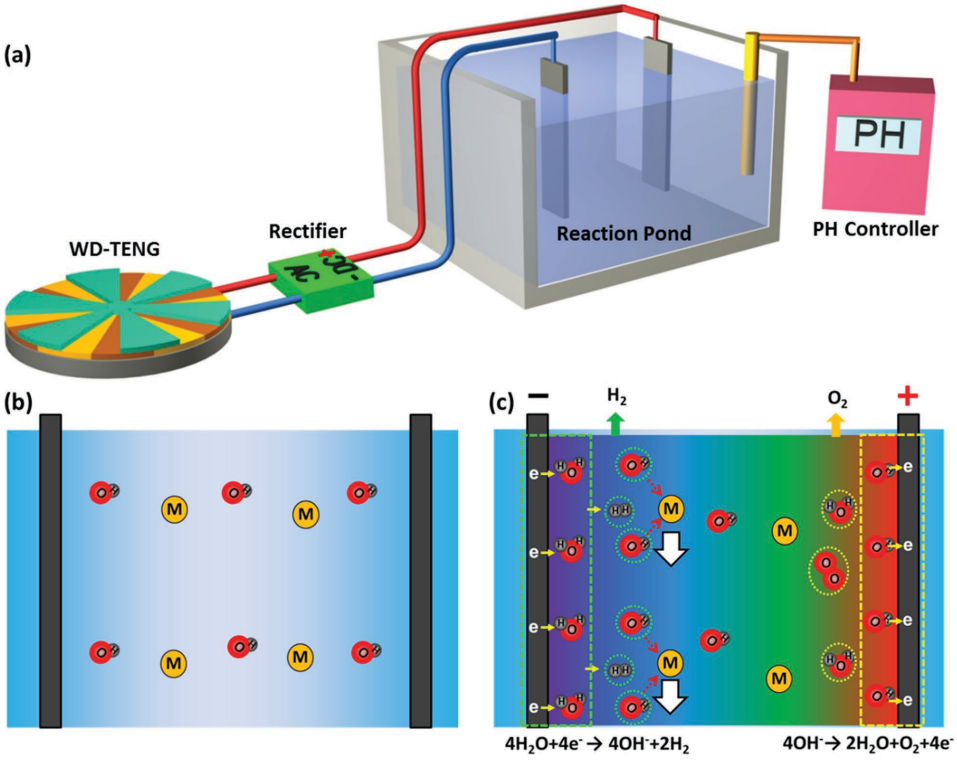

Figure 4. Working principle of the triboelectrification-enabled self-powered heavy metal ion cleaning. a) Schematic diagram of an integrated self-powered system for heavy metal ion cleaning. b) Working mechanism of the heavy metal ion precipitation process without assistance of an applied electric field. c) Proposed working mechanism showing that the heavy metal ion precipitation process was accelerated due to an applied electric field by the WD-TENG.

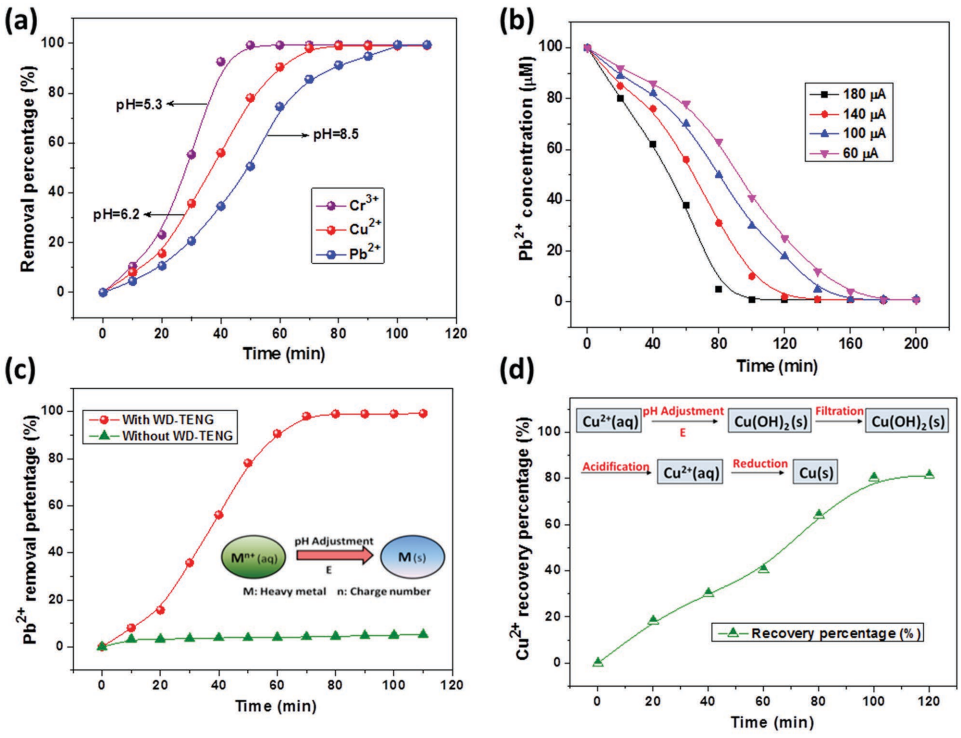

Figure 5. Performance characterization of the self-powered system for heavy metal ion removal. a) The fractional precipitation of various heavy metal ions by controlling the pH values of the wastewater. b) The output current of the WD-TENG on the removal efficiencies of Pb^{2+} in the wastewater. c) Comparison of the removal percentage of Pb^{2+} in wastewater with and without the applied electric field by the WD-TENG. The inset shows the hydroxide precipitation process of heavy metal ions under the joint action of hydroxide ions and the electric field. d) Dependence of Cu^{2+} recovery percentage on the removal time in the wastewater. The inset shows the copper metal recycling process.

Plasma-Mass Spectrometry (ICP-MS) approach was performed by using the same sample. As shown in Figure S9 in the Supporting Information, a good correlation (R^2 = 0.9983) was observed between the experimental results from two methods, which well proved the feasibility of the UV–vis approach for detecting the concentration of heavy metal ions in aqueous solution. To evaluate the performance of the self-powered integration system for heavy metal ion removal, the WD-TENG was driven at a fixed water flow rate of 3 L min^{-1}. Control experiments were carried out with or without the applied electrical field by the WD-TENG. And the UV–vis absorption spectra of the complex compound solutions, which were a mixture of the heavy metal ions and color-developing agents, are shown in Figure S10a–c in the Supporting Information. With the increasing of the operation time, the characteristic absorption peak intensity of the complex compounds, which were respectively formed by the reaction of the Cu^{2+}, Pb^{2+}, Cr^{3+} with color-developing agents in the wastewater, decreases evidently at their corresponding wavelength of 440, 510, and 540 nm, respectively. This clearly indicates the effectiveness of the route for self-powered heavy metal ion removal.

At a temperature of 25 °C, the Cu^{2+}, Pb^{2+}, and Cr^{3+} have apparently different solubility product constants (K_{sp}), as shown in Table S2 in the Supporting Information. The K_{sp} represents the maximum amount of solid that can be dissolved in the aqueous solution. The smaller the K_{sp} value of a substance, the lower is its solubility. Wastewaters from industrial processes usually contain various metal ions, and each of them has a distinct pH at which the optimum hydroxide precipitation will occur. Experimentally, by adjusting the pH value of the wastewater, using sodium hydroxide, from 5.3, 6.2, and finally to 8.5, Cr^{3+}, Cu^{2+}, and Pb^{2+} are fractionally precipitated in the forms of chromium(III) hydroxide, copper(II) hydroxide, and lead(II) hydroxide. **Figure 5**a demonstrates the removal percentage of the metal ions at each optimal pH value. As shown, the Cr^{3+} has the fastest precipitation rate, while Pb^{2+} has the slowest, which is mainly attributed to different K_{sp} values of the two, with Cr^{3+} possessing the smallest while Pb^{2+} the largest. Under a fixed current output of 0.18 mA and initial heavy metal ion concentration of 100×10^{-6} M, the self-powered cleaning system was capable of removing 97.4% of these three different heavy metal ions stepwise in the wastewater in 100 min. Also, it is worth noting that the electric output of the WD-TENG can be greatly enhanced if the self-powered cleaning system is composed of a designed multilayer configuration for practical applications. Here, thousands of single units might as well be electrically connected in parallel to form a TENG-network structure. Consequently, the voltage amplitude, the current amplitude as well as the peak density will be boosted up to a much higher level.

Furthermore, the influence of the current output on the metal ion removal performance was also studied at a fixed initial Pb^{2+} concentration of 100×10^{-6} M. As demonstrated in Figure 5b, to reach the same removal percentage, a shorter time is needed with a larger current output. Likewise, given a fixed removal time interval, a larger current output will contribute to a larger Pb^{2+} removal percentage in the wastewater. However,

Adv. Mater. **2016**,
DOI: 10.1002/adma.201504356

the residual content of the Pb^{2+} is independent of the applied current. And it remains the same in the wastewater after a continuous removal of 180 min. A further test was performed to the Cu^{2+} and Cr^{3+}, and it showed similar trends as that of the Pb^{2+}, as demonstrated in Figure S11 in the Supporting Information.

To justify the promotion of the self-provided electric field for metal ion removal, a contrast experiment was performed at a fixed initial Pb^{2+} concentration of 100×10^{-6} M. As shown in Figure 5c, and Figure S10d–f and Figure S12 in the Supporting Information, without the assistance of WD-TENG, the Pb^{2+}, Cu^{2+}, and Cr^{3+} in the wastewater show certain precipitation over time, but the removal percentage and removal efficiency are very low even though with the presence of hydroxide ions. However, with the provided electric field of the WD-TENG, the precipitation of the Pb^{2+}, Cu^{2+}, and Cr^{3+} is greatly boosted. And it largely enhanced the metal ion removal performance in term of both the required time and the removal percentage.

Admittedly, the real sewage water or wastewater is indeed very important to demonstrate the practical function of removal performance. Here, we employed the mimicked wastewater to test the effectiveness of the self-powered integration system for heavy metal ion removal. Understandably, to quantify the performance of the method, we used the mimicked wastewater with explicit metal ion categories and controlled metal ion concentrations for practical experiments. The whole detection and removal processes are physically accurate and chemically reasonable. Based on the above experimental results, it is safe and sufficient for us to verify the effectiveness and reliability of the reported self-powered detection and cleaning system.

It is important to note that microbial fuel cells (MFCs) can also be used in the water treatment process to harvest energy utilizing anaerobic digestion to collect bioenergy from wastewater. However, this kind of energy harvesting technology is mainly subjected to the organic pollutant and not applicable for the heavy metal ions. Besides, due to their intrinsic structures, MFCs can easily form biofilms and hydrocolloids during the process with time, which may largely affect the output of the energy harvesters. In comparison, the WD-TENG does not react with aqueous heavy metal ion solution directly during the removal process. The as-fabricated device was sealed thoroughly during the cleaning process to prevent the adverse influence of water/humidity on the device output. This implies that the formation of biofilm and hydrocolloids has insignificant effect on the performance of WD-TENG. The proposed substantially different approach enables unique applications in many circumstances where the usual MFCs cannot be implemented.

In addition, for recycling economic and a systematic investigation of the triboelectrification enabled self-powered heavy metal ion detection and cleaning, we also demonstrated the transformation of precipitated metal hydroxides into usable pure metals. Three procedures, including filtration, acidification, and reduction, were considered to turn the metal hydroxides into pure metals, as illustrated in the inset of Figure 5d. Copper is one example of an important and valuable metal in industrial cycles that strongly deserves to be collected and recycled. Here, taking the Cu^{2+} as an example, the Cu^{2+} recovery percentage continues to increase as the removal reaction proceeds. First, Cu^{2+} in the aqueous solution is precipitated as $Cu(OH)_2$ under the joint action of hydroxide ions and an electric filed. Then, the insoluble $Cu(OH)_2$ was filtrated to proceed the enrichment process. Subsequently, the enriched solid $Cu(OH)_2$ was acidified to dissolve Cu^{2+}, which was finally converted to pure copper metal through a chemical reduction process. The Cu^{2+} recovery percentage can reach up to 81.2% in terms of the amount of elemental copper. It is worth noting that the filtration, acidification, and reduction process were performed in the wastewater, rather than on the fabricated tribo-nanosensor or WD-TENG, which implies that the recovery process has no direct effect on the fabricated devices.

From the point of cost, on the basis of the surface charging effect, the fabrication of the device needs only very limited amounts of material, which are conventional thin-film insulating materials and metals of various kinds that are abundantly available. Besides, they have simple structures and straightforward fabrication processes. As a consequence, the developed methodology for heavy metal ion detection and removal are extremely cost-effective, which is a compelling advantage over any other wastewater treatment techniques. The presented work is a systematic and comprehensive study that could completely solve the wastewater treatment problem and it does not produce secondary pollution. In a word, with a distinctive working mechanism and rational designed device structures, the reported methodology in this work will distinguish itself in the field of wastewater treatment with unique advantages.

In summary, we introduce a fundamentally new working principle in the field of self-powered heavy metal ion detection and removal using the triboelectrification effect. By using the ligand molecules as surface modification on the AAO nanopores, the as-developed tribo-nanosensors can selectively detect common heavy metal ions, such as Cu^{2+}, Pb^{2+}, and Cr^{3+} in a sensing range of 0–200×10^{-6} M with a detection sensitivity of 0.005×10^{-6}, 0.003×10^{-6}, and 0.004×10^{-6} M^{-1}, respectively. More importantly, the triboelectrification effect was utilized to harvest the kinetic energy from wastewater flow by designing a WD-TENG, which acted as an electric power source for the heavy metal ion removal from the wastewater. Under a fixed water flow rate of 3 L min^{-1} and initial heavy metal ion concentration of 100×10^{-6} M, the integrated self-powered system was capable of removing 97.4% of the metal ions in the wastewater in 100 min. In addition, for recycling economic and a systematic investigation, the precipitated metal hydroxides were recycled and converted into usable pure metals. A recovery percentage up to 81.2% was demonstrated by calculating the amount of elemental copper. As featured with a few merits, such as environmentally friendly, cost-effective, simple with high detection sensitivity and removal efficiency, the triboelectrification-enabled heavy metal ion detection and cleaning system has potential for industrial waste management, clinical toxicology, immunological surveillance, environmental monitoring, degradation, assessment, and recycling economy.

Experimental Section

Growth of AAO Nanopores on Al Foil: With a 3% mass fraction, oxalic acid ($H_2C_2O_4$) electrolyte was employed to perform the electrochemical anodization onto the aluminum foil. The anodization was carried on

under a bias voltage of 30 V for 2.5 h with a platinum plate acting as the cathode. After that, the alumina layer was etched away in a solution of chromic acid (20 g L^{-1}) at 60 °C for 2.5 h. Then, the aluminum foil was rinsed with deionized (DI) water and dried in air.

Growth of PTFE Nanowires on PTFE Film: A PTFE film (50 μm thick) was first washed ordinally using menthol, isopropyl alcohol, and DI water. Using a DC sputter coated layer of 10 nm thickness Au onto the FEP film as a nanoscale mask for creating the surface roughness. Subsequently, the ICP reactive ion etching was applied to fabricate the aligned PTFE nanowires on the surface. O_2, Ar, and CF_4 gases were injected into the ICP chamber with a flow rate of 10.0, 15.0, and 30.0 sccm, respectively. A large density of plasma was generated by a power source of 400 W. Another power source of 100 W was used to accelerate the plasma ions. The PTFE nanowires with an approximate average length of 1.5 μm were obtained after an etching time of 40 s.

Modified AAO Nanopores with Modifying Agent: The physical adsorption method[46,47] was used to assemble a layer of modifying agent molecules onto the AAO nanopores surface as metal ions recognizing elements. At room temperature, AAO nanopores on Al substrate were immersed into the modifying agent solutions such as dithizone, diphenylcarbazide, and sodium diethyldithiocarbamate with 100×10^{-6} M concentrations for 12 h. Subsequently, the modifying agent modified AAO surface was thoroughly washed with chloroform to remove the excess of agent molecules and then dried under vacuum.

Fabrication of a Tribo-Nanosensor for Heavy Metal Ion Detection: Two pieces of acrylic with dimension of 5 cm × 5 cm were shaped by a laser cutter as the supporting substrates. Four holes were drilled at each corner for springs' installation. A layer of polydimethylsiloxane (PDMS) was covered onto the acrylic substrate, and then a layer of copper back-coated PTFE thin film was laminated onto the inner surface of the acrylic substrate as one of the contact surfaces. The Al/AAO composite was assembled onto the bottom acrylic substrate with AAO nanopores facing the PTFE on the top plate. Finally, conducting wires were connected to the Al and Cu electrodes for subsequent electrical measurements.

Fabrication of a WD-TENG: The WD-TENG mainly consists of two parts: A stator and a rotator. Stator: A square-shaped acrylic sheet was cut as a substrate with a dimension of 13 cm × 13 cm × 3 mm using a laser cutter. Through-holes on edges of the substrate were drilled for mounting it on a flat stage by screws. Fine trenches with complementary patterns were created on top of the substrate by laser cutting. A layer of Cu (200 nm) was deposited onto the substrate using an electron-beam evaporator. After that, two lead wires were connected respectively to the electrodes. A thin layer of FEP (25 μm) was finally laminated onto the electrode layer. Rotator: A disc-shaped acrylic substrate was patterned and consisted of radial-arrayed sectors by using a laser cutter. The rotator has a diameter of 10 cm and a thickness of 1.5 mm. A through-hole was drilled that has a D-profile at the centre of the rotator for a convenient connection to the water turbine. Finally, a layer of Cu (200 nm) on the rotator was deposited using a DC sputter.

Characterization and Electrical Measurement: A Hitachi SU8010 field emission scanning electron microscope, operated at 5 kV and 10 mA, was used to measure the size and shape of the grown AAO nanopores as well as the PTFE nanowires. A PANalytical X'Pert PRO diffractometer (Almelo, Netherlands) with Cu Kα radiation (λ = 0.15418 nm) was employed to measure the XRD patterns of the as-prepared AAO nanopores. The electrical signals were acquired using a programmable electrometer (Keithley Model 6514) and a low-noise current preamplifier (Stanford Research System Model SR570).

Self-Powered Integration System for Heavy Metal Ion Removal: The WD-TENG was connected to the central shaft of a miniature water turbine. Normal tap water was directed into the turbine inlet through a plastic pipe. Two pieces of graphite acting as cathode and anode were immersed in the reaction pond. A rectifying bridge was connected to output end of the WD-TENG to convert the alternating current to direct current signals. And a pH controller was employed to monitor the pH values in the reaction solution. The absorbance spectra of the complex compound solutions between heavy metal ions and color-developing agents were monitored and measured at fixed time intervals using an UV–vis spectrophotometer (JASCO V–630).

Supporting Information

Supporting Information is available from the Wiley Online Library or from the author.

Acknowledgements

Z.L. and J.C. contributed equally to this work. The research was supported by the U.S. Department of Energy, Office of Basic Energy Sciences, Division of Materials Sciences and Engineering under Award DE-FG02-07ER46394, the Hightower Chair Foundation, and the "thousands talents" program for pioneer researcher and his innovation team, China, the National Natural Science Foundation of China (Grant No. 51432005), and the Beijing City Committee of Science and Technology (Z131100006013004 and Z131100006013005).

Received: September 5, 2015
Revised: December 17, 2015
Published online:

[1] F. Fu, Q. Wang, *J. Environ. Manage.* **2011**, *92*, 407.
[2] C.-T. Chen, W.-P. Huang, *J. Am. Chem. Soc.* **2002**, *124*, 6246.
[3] J.-S. Hu, L.-S. Zhong, W.-G. Song, L.-J. Wan, *Adv. Mater.* **2008**, *20*, 2977.
[4] K. Rurack, M. Kollmannsberger, U. Resch-Genger, J. Daub, *J. Am. Chem. Soc.* **2000**, *122*, 968.
[5] E. S. Forzani, H. Zhang, W. Chen, N. Tao, *Environ. Sci. Technol.* **2005**, *39*, 1257.
[6] D. T. Quang, J. S. Kim, *Chem. Rev.* **2010**, *110*, 6280.
[7] Q. He, E. W. Miller, A. P. Wong, C. J. Chang, *J. Am. Chem. Soc.* **2006**, *128*, 9316.
[8] A. Yuchi, T. Sato, Y. Morimoto, H. Mizuno, H. Wada, *Anal. Chem.* **1997**, *69*, 2941.
[9] Y. Kim, R. C. Johnson, J. T. Hupp, *Nano Lett.* **2001**, *1*, 165.
[10] A. El-Rehim, H. A. Hegazy, E. A. Ali, A. El-Hag, *React. Funct. Polym.* **2000**, *43*,105.
[11] A. Dabrowski, Z. Hubicki, P. Podkoscielny, E. Robens, *Chemosphere* **2004**, *56*, 91.
[12] Z. Wang, M. Wang, G. Wu, D. Wu, A. Wu, *Dalton Trans.* **2014**, *43*, 8461.
[13] S. Wang, E. S. Forzani, N. Tao, *Anal. Chem.* **2007**, *79*, 4427.
[14] Y. Suzuki, *IEEJ Trans. Electr. Electron. Eng.* **2011**, *6*, 101.
[15] H. W. Lo, Y. C. Tai, *J. Micromech. Microeng.* **2008**, *18*, 104006.
[16] R. Tashiro, N. Kabei, K. Katayama, E. Tsuboi, *J. Artif. Organs* **2002**, *5*, 239.
[17] J. Chen, G. Zhu, W. Yang, Q. Jing, P. Bai, Y. Yang, T. C. Hou, Z. L. Wang, *Adv. Mater.* **2013**, *25*, 6094.
[18] G. Zhu, J. Chen, Y. Liu, P. Bai, Y. Zhou, Q. Jing, C. Pan, Z. L. Wang, *Nano Lett.* **2013**, *13*, 2282.
[19] G. Zhu, J. Chen, T. Zhang, Q. Jing, Z. L. Wang, *Nat. Commun.* **2014**, *5*, 3426.
[20] W. Yang, J. Chen, G. Zhu, X. Wen, P. Bai, Y. Su, Y. Lin, Z. L. Wang, *Nano Res.* **2013**, *6*, 880.
[21] J. Chen, J. Yang, H. Guo, Z. Li, L. Zheng, Y. Su, Z. Wen, X. Fan, Z. L. Wang, *ACS Nano* **2015**, *9*, 11688.
[22] P. D. Mitcheson, P. Miao, B. H. Stark, E. M. Yeatman, A. S. Holmes, T. C. Green, *Sens. Actuator, A* **2004**, *115*, 523.
[23] Z. L. Wang, J. Chen, L. Lin, *Energy Environ. Sci.* **2015**, *8*, 2250.

[24] Y. Suzuki, D. Miki, M. Edamoto, M. Honzumi, *J. Micromech. Microeng.* **2010**, *20*, 104002.
[25] J. Chen, G. Zhu, J. Yang, Q. Jing, P. Bai, W. Yang, X. Qi, Y. Su, Z. L. Wang, *ACS Nano* **2015**, *9*, 105.
[26] W. Yang, J. Chen, G. Zhu, J. Yang, P. Bai, Y. Su, Q. Jing, Z. L. Wang, *ACS Nano* **2013**, *7*, 11317.
[27] X. Fan, J. Chen, J. Yang, P. Bai, Z. Li, Z. L. Wang, *ACS Nano* **2015**, *9*, 4236.
[28] J. Yang, J. Chen, Y. Su, Q. Jing, Z. Li, F. Yi, X. Wen, Z. Wang, Z. L. Wang, *Adv. Mater.* **2015**, *27*, 1316.
[29] H. Guo, J. Chen, M. H. Yeh, X. Fan, Z. Wen, Z. Li, C. Hu, Z. L. Wang, *ACS Nano* **2015**, *9*, 5577.
[30] Z. Li, J. Chen, J. Yang, Y. Su, X. Fan, Y. Wu, C. Yu, Z. L. Wang, *Energy Environ. Sci.* **2015**, *8*, 887.
[31] Y. Su, J. Chen, Z. Wu, Y. Jiang, *Appl. Phys. Lett.* **2015**, *106*, 013114.
[32] J. Yang, J. Chen, Y. Liu, W. Yang, Y. Su, Z. L. Wang, *ACS Nano* **2014**, *8*, 2649.
[33] J. Yang, J. Chen, Y. Yang, H. Zhang, W. Yang, P. Bai, Y. Su, Z. L. Wang, *Adv. Energy Mater.* **2014**, *4*, 1301322.
[34] J. Chen, J. Yang, Z. Li, X. Fan, Y. Zi, Q. Jing, H. Guo, Z. Wen, K. C. Pradel, S. Niu, Z. L. Wang, *ACS Nano* **2015**, *9*, 3324.
[35] G. Zhu, Y. Su, P. Bai, J. Chen, Q. Jing, W. Yang, Z. L. Wang, *ACS Nano* **2014**, *8*, 6031.
[36] W. Yang, J. Chen, Q. Jing, J. Yang, X. Wen, Y. Su, G. Zhu, P. Bai, Z. L. Wang, *Adv. Funct. Mater.* **2014**, *24*, 4090.
[37] W. Yang, J. Chen, X. Wen, Q. Jing, J. Yang, Y. Su, G. Zhu, W. Wu, Z. L. Wang, *ACS Appl. Mater. Interfaces* **2014**, *6*, 7479.
[38] W. Tang, Y. Han, C. Han, C. Gao, X. Cao, Z. L. Wang, *Adv. Mater.* **2015**, *27*, 272.
[39] Z.-H. Lin, G. Zhu, Y. S. Zhou, Y. Yang, P. Bai, J. Chen, Z. L. Wang, *Angew. Chem. Int. Ed.* **2013**, *52*, 1.
[40] H. Zhu, W. Tang, C. Gao, Y. Han, T. Li, X. Cao, Z. L. Wang, *Nano Energy* **2015**, *14*, 193.
[41] S. Chen, C. Gao, W. Tang, H. Zhu, Y. Han, Q. Jiang, T. Li, X. Cao, Z. L. Wang, *Nano Energy* **2015**, *14*, 217.
[42] Y. Su, G. Zhu, W. Yang, J. Yang, J. Chen, Q. Jing, Z. Wu, Y. Jiang, Z. L. Wang, *ACS Nano* **2014**, *8*, 3843.
[43] Z.-H. Lin, G. Cheng, L. Lin, S. Lee, Z. L. Wang, *Angew. Chem. Int. Ed.* **2013**, *52*, 12545.
[44] World Health Organization, *Guidelines for Drinking-Water Quality*, Geneva, Switzerland **2011**.
[45] World Health Organization, *International Scheme to Evaluate Household Water Treatment Technologies-Harmonized Testing Protocol: Technology Non-Specific*Geneva, Switzerland **2014**.
[46] H. Choi, S. O. Kang, J. Ko, G. Gao, H. S. Kang, M.-S. Kang, M. K. Nazeeruddin, M. Grätzel, *Angew. Chem. Int. Ed.* **2009**, *48*, 5938.
[47] J. M. Notestein, E. Iglesia, A. Katz, *J. Am. Chem. Soc.* **2004**, *126*, 16478.